Coupled Magnetic Cycloids in Multiferroic TbMnO_{3} and Eu_{3/4}Y_{1/4}MnO_{3}

Hoyoung Jang, J.-S. Lee, K.-T. Ko, W.-S. Noh, T. Y. Koo, J.-Y. Kim, K.-B. Lee, J.-H. Park, C. L. Zhang, Sung Baek Kim, and S.-W. Cheong

Coupled Magnetic Cycloids in Multiferroic TbMnO$_3$ and Eu$_{3/4}$Y$_{1/4}$MnO$_3$

Hoyoung Jang,[1] J.-S. Lee,[1,*] K.-T. Ko,[1] W.-S. Noh,[1] T. Y. Koo,[2] J.-Y. Kim,[2] K.-B. Lee,[2,1] J.-H. Park,[1,2,3,†] C. L. Zhang,[4] Sung Baek Kim,[5,‡] and S-W. Cheong[4,5]

[1]*Department of Physics, Pohang University of Science and Technology, Pohang 790-784, Korea*

[2]*Pohang Acceleration Laboratory, Pohang University of Science and Technology, Pohang 790-784, Korea*

[3]*Division of Advanced Materials Science, Pohang University of Science and Technology, Pohang 790-784, Korea*

[4]*R-CEM & Department of Physics and Astronomy, Rutgers University, Piscataway, NJ 08854, USA*

[5]*l_PEM & Department of Physics, Pohang University of Science and Technology, Pohang 790-784, Korea.*

Abstract

Based on the detailed Mn $L_{2,3}$-edge x-ray resonant scattering results, we report new complexity in the magnetic order of multiferroic orthomangnites, which has been widely considered as the simple A-type cycloid order inducing ferroelectricity. The Dzyaloshinskii-Moriya interaction involved in the orthorhombic distortion brings on F-type canting of the A-type ordered spin, and the ordering type becomes the off-phase synchronized bc-cycloid in TbMnO$_3$ or the tilted anti-phase ab-cycloid in Eu$_{3/4}$Y$_{1/4}$MnO$_3$. The F-type, which is a ferro-type along the c-axis, is responsible for the magnetic field-driven multiferroicity to weak ferromagnetism transition.

PACS numbers: 75.85.+t, 75.25.-j, 78.70.Ck, 75.30.Et

Discovery of large magnetoelectric effects in orthomanganite $TbMnO_3$ [1] stimulated tremendous studies of multiferroicity [2, 3], in which ferroelectricity and magnetism are intimately coupled, due to its great technological and fundamental importance. The magnetoelectric effects were found to be greatly enhanced especially in spiral/cycloid magnetic systems [3–6] and the noncollinear cycloid magnetism became one of the most important issues in the multiferroicity. The ferroelectricity in the magnetic cycloid is induced by unidirectional shifts of the oxygen ions to obtain an energy gain through animating Dzyaloshinskii-Moriya (DM) interaction [7, 8], the so called *inverse* DM interaction [9]. Then the relationship between the magnetic cycloid and the electric polarization was explained in the spin current model [10].

$TbMnO_3$, a prototype magnetic cycloid ferroelectric system, was reported to display a variety of magnetic and electric properties [4, 11–13]. Below $T_N \approx 42$ K, the system has an incommensurate A-type b-sinusoid order, where collinear spins on the b-axis with antiparallel neighboring alignment along the c-axis (A-type) modulate along the b-axis with a wavevector $\vec{q} = q\hat{b}$ ($q \sim 0.28$). Upon cooling through $T_C \approx 28$ K, it transits into the A-type bc-plane spin cycloid (bc-cycloid) inducing ferroelectricity with electric polarization $\vec{P} = P_c\hat{c}$. The spin chirality is reversed by switching the polarization [14]. A magnetic field $\vec{H} = H_b\hat{b}$ (~ 5 T) switches the bc-cycloid into the ab-plane spin cycloid (ab-cycloid) with $\vec{P} = P_a\hat{a}$ [12, 15]. The ab-cycloid can be also realized by changing the rare-earth ions as in $(Eu,Y)MnO_3$ [16, 17] and $(Gd,Tb)MnO_3$ [18]. On the other hand, the system undergoes a first order transition into a weak ferromagnet in $\vec{H} = H_c\hat{c}$ (< 12 T) below T_C [12, 16], resulting in intriguing field induced cross-controls of magnetization and electric polarization [16].

The DM interaction was originally introduced to explain weak ferromagnetism (FM) in antiferromagnets, resulting from uniaxial F-type spin canting due to structural zig-zag type ligand shifts [7, 8]. Indeed, the weak FM was observed in orthorhombic $LaMnO_3$ [19], in which the DM interaction of the zig-zag type shifts in Mn-O-Mn chains induces the F-type spin canting in the A-type antiferromagnetic (AFM) order. Then the DM interaction is often considered to originate either the spiral ferroelectricity or the canted weak FM in the orthomanganites [2]. However considering that the orthorhombic perovskite commonly possesses the zig-zag type shifts, one can raise fundamental issues on the magnetic structure of the multiferroic orthomanagnite; how the F-type canting is integrated into the A-type cycloid and which magnetic structure results from a combination of the inverse and ordinary

2

DM interactions. Those are schematically addressed in a scenario described in Fig. 1.

Let us consider a Mn-O-Mn chain along the c-axis with a transverse oxygen shift $\vec{x} = x\hat{b}$ due to the orthorhombic distortion as shown in Fig. 1(a). The superexchange interaction $H_{SE} = J\vec{S}_i \cdot \vec{S}_j$ $(J > 0)$ makes the neighboring Mn spins, S_i and S_j, antiparallel to each other, resulting in the A-type order. The oxygen shift $\vec{x}$ induces the DM interaction $H_{DM} = \vec{D} \cdot \vec{S}_i \times \vec{S}_j$ through the Dzyaloshinskii D vector $\vec{D} = \lambda\vec{x} \times \hat{r}_{ij}$, where λ denotes the spin-orbit coupling constant and $\hat{r}_{ij}$ is a unit vector from S_i to S_j [2, 7–9]. In the A-type b-sinusoid with $\vec{q} = q\hat{b}$, all spins lie on the b-axis, and the local magnetic moments can be described by $\vec{m}_i^A = m_b^A \cos(\vec{q} \cdot \vec{r}_i)\hat{b}$, while in the A-type bc- and ab-cycloids with the spins in the bc- and ab-planes, they can be by $\vec{m}_i^A = m_b^A \cos(\vec{q} \cdot \vec{r}_i)\hat{b} + m_c^A \sin(\vec{q} \cdot \vec{r}_i)\hat{c}$ and $\vec{m}_i^A = m_b^A \cos(\vec{q} \cdot \vec{r}_i)\hat{b} + m_a^A \sin(\vec{q} \cdot \vec{r}_i)\hat{a}$, respectively [14]. The zig-zag type shifts $\vec{x} = \pm x\hat{b}$ yield $\vec{D} = \pm D\hat{a}$. H_{DM} acts only on m_b^A and m_c^A, and contributes the F-type spin canting to the c- and b-directions, respectively, but not on m_a^A, i.e. $m_b^A \rightarrow m_c^F$, $m_c^A \rightarrow -m_b^F$, $m_a^A \rightarrow 0$. Then, the F-type order due to the spin canting is predicted to be the c-sinusoid $\vec{m}_i^F = m_c^F \cos(\vec{q} \cdot \vec{r}_i)\hat{c}$ (Fig. 1(b)) or the bc-cycloid $\vec{m}_i^F = -m_b^F \sin(\vec{q} \cdot \vec{r}_i)\hat{b} + m_c^F \cos(\vec{q} \cdot \vec{r}_i)\hat{c}$ (Fig. 1(c)) for the A-type b-sinusoid or bc-cycloid, respectively. For the A-type ab-cycloid, the F-type order is the c-sinusoid $\vec{m}_i^F = m_c^F \cos(\vec{q} \cdot \vec{r}_i)\hat{c}$ (Fig. 1(d) since $m_a^A \rightarrow 0$. It is noticeable that the F-type is synchronized to the A-type with the same $\vec{q}(= q\hat{b})$ and chirality. Then, in the A-type bc-cycloid case (Fig. 1(e)), the net spin structure, the sum of the A-type and F-type components, becomes the *off-phase synchronized* cycloid with the phase difference between the c-axis neighboring spins changing from π to $\pi \pm 2\phi$ due to the unidirectional F-type canting angle ϕ of $\tan\phi \approx |D|/2J$. In the A-type ab-cycloid case (Fig. 1(f)), it becomes the *tilted anti-phase* cycloid with the cycloid planes tilted by $\pm\phi$.

To examine the scenario, we scrutinized the F-type orders in TbMnO$_3$ (A-type bc-cycloid) and Eu$_{3/4}$Y$_{1/4}$MnO$_3$ (A-type ab-cycloid) using the Mn $L_{2,3}$-edge $(2p \rightarrow 3d)$ x-ray resonant scattering (XRS) in full combinations of the scattering geometry and the in-coming photon polarization at the 2A beamline in Pohang Light Source (PLS) [20]. TbMnO$_3$ and Eu$_{3/4}$Y$_{1/4}$MnO$_3$ single crystals were grown by a floating zone method [4, 16]. After cut along the (010) plane and polished, the crystals were annealed for the surface recovery. The electrical polarization $\vec{P}$ and the chirality $\vec{C} = \sum \vec{S}_n \times \vec{S}_{n+1}$ were reversed above T_N ($\approx$ 50K) by an electric field ($\approx \pm$1kV/mm) along $\hat{c}$ for TbMnO$_3$ ($\vec{P} = \pm P_c\hat{c}$) and along $\hat{a}$ for Eu$_{3/4}$Y$_{1/4}$MnO$_3$ ($\vec{P} = \pm P_a\hat{a}$) [14]. After field cooled, XRS measurements were performed

3

with warming at given temperatures maintained within 0.1 K. In the Mn K-edge ($1s \rightarrow 4p$) XRS, the F-type (0 4$-q$ 0) reflection peak appeared at the same q as the A-type (0 4$-q$ 1) one. However it is rather vague due to its weak intensity, about two orders of magnitude smaller than that of the A-type [21], and it has been disputed whether the origin is an intrinsic magnetic order [22]. On the other hand, such small intensity is consistent with the small F-type ordered moment expected in the DM induced canted spin. The Mn $L_{2,3}$-edge XRS, which directly accesses to the magnetic $3d$ states, enhances the reflection by roughly four orders of magnitude and enables us to make full investigations on the F-type behaviors.

Figure 2 shows the experimental geometry and the Mn $L_{2,3}$-edge XRS energy profile of the F-type (0 q 0) reflection for TbMnO$_3$ ($q \approx 0.28$) and Eu$_{3/4}$Y$_{1/4}$MnO$_3$ ($q \approx 0.25$) at 10 K in comparison with the x-ray absorption spectroscopy (XAS) spectra, which display the clean Mn^{3+} one to verify the surface quality. Both q-values slightly increase above T_C [21]. The energy profile exhibits nearly identical line shape for both systems without noticeable temperature dependence. The k-scan shown in the inset clearly displays the F-type reflection peak. Its coherence length, which can be extracted from the peak width, turns out to be about the same as that of the A-type [21], implying that both A- and F-types may originate from a single magnetic order. The elliptically polarized undulator beamline with full selectivity of the photon polarization enables us to perform the XRS measurements for four different photon polarizations, the vertical (σ) and planar (π) linear and the right (R) and left (L) circular, without change in the geometry.

The predicted F-type order, either the *cycloid* or the *sinusoid*, can be directly examined in XRS by using the circularly polarized light. As demonstrated previously [23], the XRS intensity for the magnetic cycloid varies with the incoming photon *helicity* vector parallel or antiparallel to the spin chirality $\vec{C}$ to yield circular dichoism. Indeed, XRS in the ab-plane scattering exhibits large circular dichroism at the F-type reflection for TbMnO$_3$ (A-type bc-cycloid) at 10 K ($< T_C \approx 28$ K) as shown in Fig. 3(a). The dichroism is reversed with $\vec{P}$ switching ($\pm P_c \hat{c}$), which accompanies chirality reversal of the A-type cycloid [14], meaning the simultaneous chirality reversal (synchronized coupling) of the A-type and F-type cycloids. The dichroism gradually reduces upon heating and vanishes above T_C although the F-type signal still survives up to $T_N \approx 42$ K as shown in Fig. 3(b) [24]. No dichroism, however, was observed in the bc-plane scattering even below T_C [21], meaning $m_a^F \simeq 0$ in the cycloid. These results manifest that the F-type is the noncollinear bc-cycloid below T_C with

4

the chirality reversal and becomes the collinear c-sinusoid above T_C up to T_N, in contrast to a recent proposal [25] that the F-type is sinusoidal below T_C (see Ref. [26] for additional information). Meanwhile in $Eu_{3/4}Y_{1/4}MnO_3$ (A-type ab-cycloid), the F-type reflection does not show any considerable circular dichroism, regardless of the scattering plane as shown in Fig. 3(c), proving that the F-type is sinusoidal even below T_C. It is worth to note that all the observed F-type orders agree with the magnetic symmetry arguments, which can be described in the irreducible representations for the propagation vector $\vec{G}_k = (0, k, 0)$ in the space group $Pbnm$ of the $GdFeO_3$-type distorted orthomanganites [27]. Further, the representations tell that the system also allows the G- and C-type magnetic structures [21] and suggest that the true spin structure can be a multi-faced structure displaying different types of the ordering structure possibly observed at different reflections [11].

The spin cycloid and the chirality are directly examined in XRS with circularly polarized light, but XRS with linearly (σ and π) polarized light is necessary for quantitative analysis of the ordered local magnetic moment. Figure 4 shows the ab-plane scattering results. In $TbMnO_3$ (A-type bc-cycloid), the F-type reflection yields significantly enhanced $I(\pi)$ but negligible $I(\sigma)$ at $T = 30$ K ($> T_C$), while at $T = 10$ K ($< T_C$), both $I(\pi)$ and $I(\sigma)$ become finite. In $Eu_{3/4}Y_{1/4}MnO_3$ (A-type ab-cycloid), it shows large $I(\pi)$ but no $I(\sigma)$ both above and below T_C. Such intensity variations can be explained by the magnetic scattering amplitude for the electric dipole transition [28, 29].

In the ab-plane scattering for a modulated ($\vec{q} = q\hat{b}$) magnetic order with the chirality $\hat{C} = \pm\hat{a}$ and scattering angle θ, the magnetic scattering intensities $I(\sigma)$, $I(\pi)$, $I(R)$, and $I(L)$ for the respective photon polarizations σ, π, R, and L can be represented as [30]

$$I(\sigma) = m_a^2 \cos^2\theta + m_b^2 \sin^2\theta,$$

$$I(\pi) = m_a^2 \cos^2\theta + m_b^2 \sin^2\theta + m_c^2 \sin^2 2\theta,$$

$$I(R) = (I(\sigma) + I(\pi))/2 \mp m_b m_c \sin\theta \sin 2\theta,$$

$$I(L) = (I(\sigma) + I(\pi))/2 \pm m_b m_c \sin\theta \sin 2\theta.$$

Here m_a, m_b, and m_c are the a-, b-, and c-axis maximum components of the local magnetic moment respectively. Above T_C, the F-type in $TbMnO_3$ is the c-sinusoid, $\vec{m}_i^F = m_c^F \cos(\vec{q} \cdot \vec{r}_i)\hat{c}$, which yields finite $I(\pi)$ but no $I(\sigma)$. Below T_C, it becomes the bc-cycloid, $\vec{m}_i^F = -m_b^F \sin(\vec{q} \cdot \vec{r}_i)\hat{b} + m_c^F \cos(\vec{q} \cdot \vec{r}_i)\hat{c}$ with finite $I(\pi)$ and $I(\sigma)$. With $\theta \approx 27°$, the ratio m_b^F/m_c^F is estimated to be about 0.7, simply inverse to that in the A-type bc-cycloid [14], i.e. $m_b^F/m_c^F \approx$

m_c^A/m_b^A (ellipticity reversal). These results absolutely agree with the scenario for the F-type spin canting driven by the DM interaction of $\vec{D} = \pm D\hat{a}$, which makes contributions of $m_b^A \to m_c^F$ and $m_c^A \to -m_b^F$. The temperature dependence of both m_b^F and m_c^F, extracted from $I(\sigma)$ and $I(\pi)$, agrees well with the simple power law $(T_N - T)^{1/2}$. $m_b^F/m_c^F \approx 0.7$ also reproduces the temperature dependence for $I(R)$ and $I(L)$ (see Fig. 3(b)). In $\mathrm{Eu_{3/4}Y_{1/4}MnO_3}$ with m_a^A and m_b^A, the F-type maintains the c-sinusoid even below T_C since $m_a^A \to 0$ and $m_b^A \to m_c^F$. Thus XRS shows a finite intensity only for $I(\pi)$, and $\left|m_c^F\right|^2$ is roughly proportional to $I(\pi)$ (see Fig. 4(e)). We also note that in the bc-plane scattering, the F-type reflection intensity shows no noticeable variation for different photon polarizations in both systems above and below T_C, i.e. the same intensity for $I(\sigma)$, $I(\pi)$, $I(R)$, and $I(L)$ [21], confirming that the F-type involves $\vec{D} = \pm D\hat{a}$ and $m_a^F = 0$.

Considering that the oxygen shifts $\vec{x} = \pm x\hat{b}$ inducing the F-type originate the weak FM in the collinear A-type AFM $\mathrm{LaMnO_3}$ [19], one expects that the weak FM can be also realized in the multiferroic orthomanganites when the cycloid is released, similarly with a field driven spin structure transition in $\mathrm{BiFeO_3}$ [31]. Indeed, a sufficiently large $\vec{H} = H_c\hat{c}$ derives a first order *unwinding* transition into the weak FM state in $\mathrm{TbMnO_3}$ [12] and $\mathrm{Eu_{3/4}Y_{1/4}MnO_3}$ [16], where the collinear A-type AFM order is stabilized and the ferroelectricity disappears. The respective ferromagnetic moments are obtained to be $0.27 \pm 0.02\mu_B/\mathrm{Mn}$ and $0.18 \pm 0.02\mu_B/\mathrm{Mn}$ at 10 K [21], which are slightly larger than and comparable to the moment $0.18\mu_B/\mathrm{Mn}$ for $\mathrm{LaMnO_3}$ [19]. The first order type hysteresis behavior observed at the transition implies possible coexistence of the competing two phases, and the F-type makes intriguing field induced cross-controls of ferroelectricity and ferromagnetism possible [16].

In summary, we clarified the F-type magnetic orders coupled to the A-type ones in multiferroic orthomanganites using the Mn $L_{2,3}$-edge XRS studies. The F-type induced by the DM interaction is either a cycloid or sinusoid, resulting in novel spin structures.

* present address: NSLS Brookhaven National Laboratory, Upton, NY 11973

† Author to whom all correspondences should be addressed. e-mail: jhp@postech.ac.kr

‡ present address: Department of Physics, Kookmin University, Seoul 136-702, Korea

[1] T. Kimura *et al.*, Nature (London) **426**, 55 (2003).

[2] S-W. Cheong and M. Mostovoy, Nat. Mater. **6**, 13 (2007).

[3] T. Kimura, Annu. Rev. Mater. Res. **37**, 387 (2007).

[4] M. Kenzelmann *et al.*, Phys. Rev. Lett. **95**, 087206 (2005).

[5] G. Lawes *et al.*, Phys. Rev. Lett. **95**, 087205 (2005).

[6] K. Taniguchi *et al.*, Phys. Rev. Lett. **97**, 097203 (2006).

[7] I. Dzyaloshinskii, J. Phys. Chem. Solids **4**, 241 (1958).

[8] T. Moriya, Phys. Rev. **120**, 91 (1960).

[9] I. A. Sergienko and E. Dagotto, Phys. Rev. B **73**, 094434 (2006).

[10] H. Katsura, N. Nagaosa, and A. V. Balatsky, Phys. Rev. Lett. **95**, 057205 (2005).

[11] R. Kajimoto *et al.*, Phys. Rev. B **70**, 012401 (2004).

[12] T. Kimura *et al.*, Phys. Rev. B **71**, 224425 (2005).

[13] N. Abe *et al.*, Phys. Rev. Lett. **99**, 227206 (2007).

[14] Y. Yamasaki *et al.*, Phys. Rev. Lett. **98**, 147204 (2007); *ibid* **100**, 219902(E) (2008).

[15] N. Aliouane *et al.*, Phys. Rev. Lett. **102**, 207205 (2009).

[16] Y. J. Choi *et al.*, Phys. Rev. Lett. **105**, 097201 (2010).

[17] J. Hemberger *et al.*, Phys. Rev. B **75**, 035118 (2007).

[18] Y. Yamasaki *et al.*, Phys. Rev. Lett. **101**, 097204 (2008).

[19] V. Skumryev *et al.* Eur. Phys. J. B **11**, 401 (1999).

[20] J.-S. Lee *et al.*, J. Kor. Phys. Soc. **52**, 1814 (2008).

[21] H. Jang *et al.* unpublished.

[22] D. Mannix *et al.*, Phys. Rev. B **76**, 184420 (2007).

[23] J. C. Lang, D. R. Lee, D. Haskel, and G. Srajer, J. Appl. Phys. **95**, 6537 (2004).

[24] The small dichroism size difference with the E reversal may be due to experimental artifacts such as incomplete chirality reversal and/or small difference in degree of circular polariation (Ref.[26] for additional information).

[25] S. B. Wilkins *et al.*, Phys. Rev. Lett. **103**, 207602 (2009).

[26] See supplementary materials.

[27] H. W. Brinks *et al.* Phys. Rev. B **63**, 94411 (2001).

[28] J. P. Hannon, G. T. Trammell, M. Blume, and D. Gibbs, Phys. Rev. Lett. **61**, 1245 (1988).

[29] J. P. Hill and D. F. McMorrow, Acta Cryst.**A52**, 236 (1996).

[30] S. W. Lovesey and S. P. Collins, Scattering and Absorption by Magnetic Materials (Clarendon, Oxford, 1996).

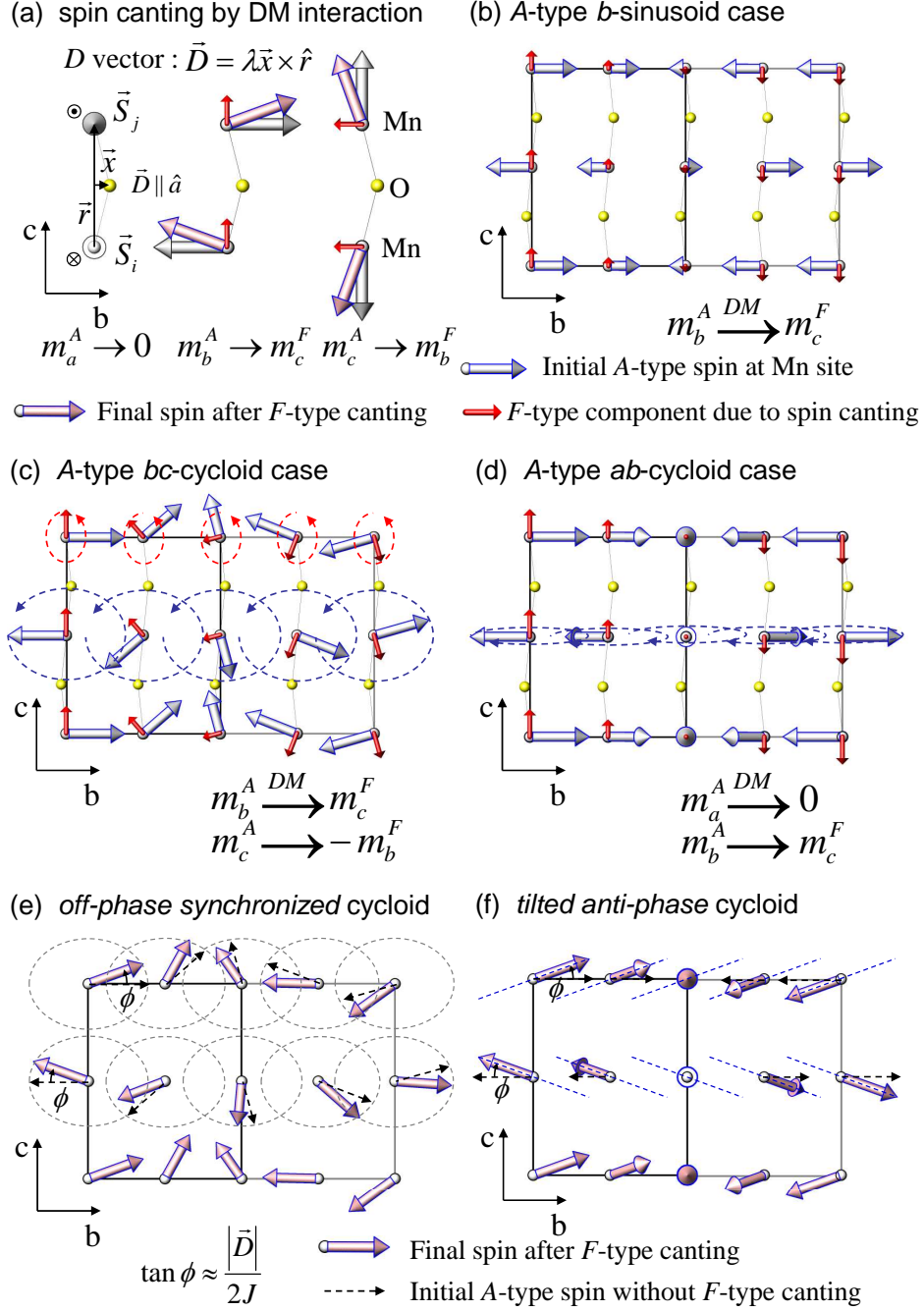[31] B. Ruette *et al.*, Phys. Rev. B **69**, 064114 (2004).

(a) spin canting by DM interaction

D vector : $\vec{D} = \lambda \vec{x} \times \hat{r}$

$\vec{S}_j$

$\vec{x}$

$\vec{D} \parallel \hat{a}$

$\vec{r}$

$\vec{S}_i$

Mn

O

Mn

$m_a^A \to 0 \quad m_b^A \to m_c^F \quad m_c^A \to m_b^F$

(b) A-type b-sinusoid case

$m_b^A \xrightarrow{DM} m_c^F$

Initial A-type spin at Mn site

Final spin after F-type canting

F-type component due to spin canting

(c) A-type bc-cycloid case

$m_b^A \xrightarrow{DM} m_c^F$

$m_c^A \longrightarrow -m_b^F$

(d) A-type ab-cycloid case

$m_a^A \xrightarrow{DM} 0$

$m_b^A \longrightarrow m_c^F$

(e) *off-phase synchronized* cycloid

ϕ

ϕ

$\tan\phi \approx \dfrac{|\vec{D}|}{2J}$

(f) *tilted anti-phase* cycloid

ϕ

ϕ

Final spin after F-type canting

Initial A-type spin without F-type canting

FIG. 1: (a) Spin canting by the DM interaction inducing F-type components m_c^F and m_b^F from the A-type m_b^A and m_c^A, respectively, but no F-type from m_a^A. (b)-(d) Induced F-type c-sinusoid, bc-cycloid, and c-sinusoid for the A-type b-sinusoid, bc-cycloid, and ab-cycloid, respectively. Resulting net spin stuctures; (e) *off-phase* synchronized cycloid and (f) *tilted anti-phase* cycloid.
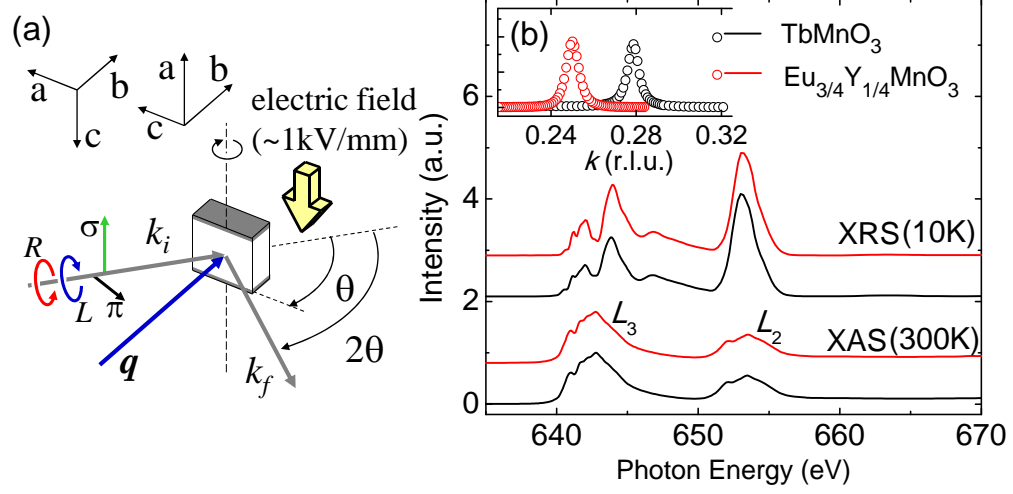
9

FIG. 2: (a) Scattering geometries on the bc- and ab-planes. (b) XRS energy profiles compared with the XAS spectra of $TbMnO_3$ and $Eu_{3/4}Y_{1/4}MnO_3$. The inset shows the F-type reflection peaks ($h\nu = 653$ eV) along (0 k 0).
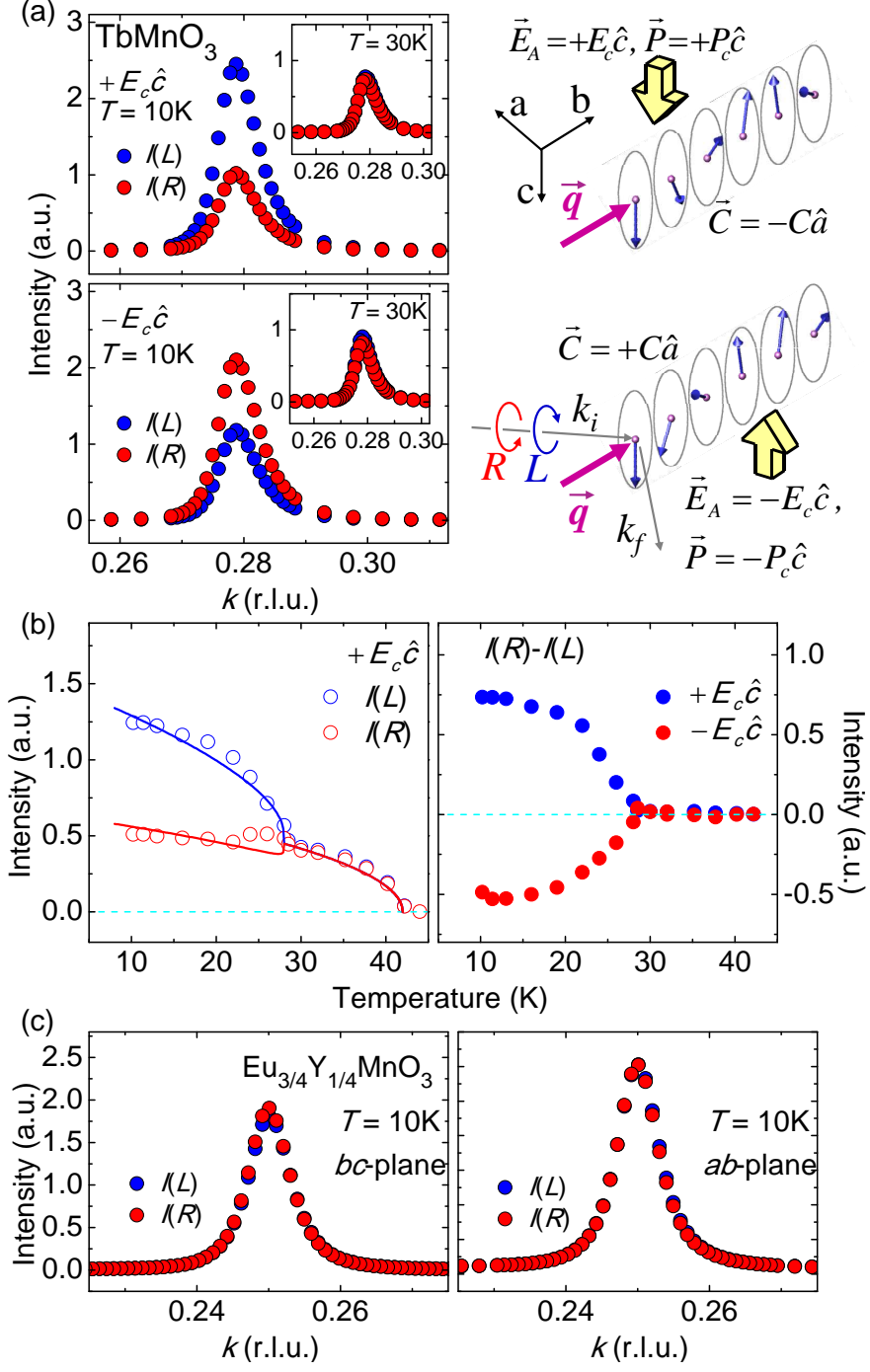
FIG. 3: (a) $I(L)$ and $I(R)$ along $(0\ k\ 0)$ in the ab-plane scattering at $h\nu = 653$ eV for E-fields $\vec{E}_A = \pm E_c\hat{c}$, and (b) temperature dependence of $I(L)$ and $I(R)$ compared with calculations (solid lines) by using m_b^F and m_c^F in Fig. 4(c) and of $I(L) - I(R)$ of TbMnO$_3$. (c) $I(L)$ and $I(R)$ along $(0\ k\ 0)$ in the bc- and ab-plane scattering of Eu$_{3/4}$Y$_{1/4}$MnO$_3$.
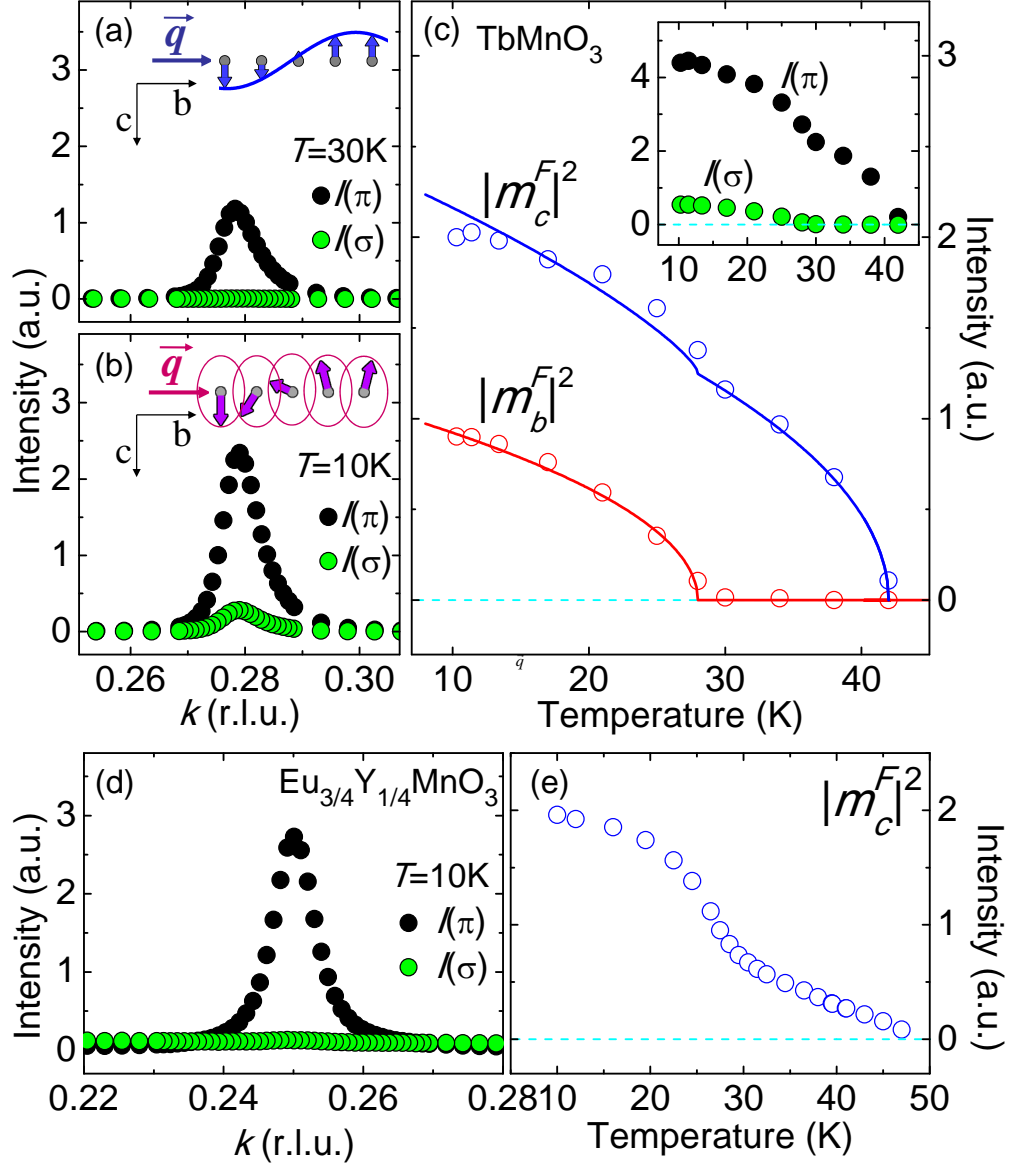
11

FIG. 4: The *ab*-plane scattering at $h\nu = 653$ eV. (a) *k*-scan $I(\pi)$ and $I(\sigma)$ at 30 K, (b) at 10 K, and (c) temperature dependence of $\left|m_c^F\right|^2$ and $\left|m_b^F\right|^2$ (open circles) extracted from $I(\pi)$ and $I(\sigma)$ (Inset) are compared with simple power law fits (solid lines) of $TbMnO_3$. (d) *k*-scan $I(\pi)$ and $I(\sigma)$ at 10 K and (e) temperature dependence of extracted $\left|m_c^F\right|^2$ of $Eu_{3/4}Y_{1/4}MnO_3$.